IOPscience iopscience.iop.org

Home Search Collections Journals About Contact us My IOPscience

Lift crisis of a spinning table tennis ball

This content has been downloaded from IOPscience. Please scroll down to see the full text.

2017 Eur. J. Phys. 38 024001

(http://iopscience.iop.org/0143-0807/38/2/024001)

View the table of contents for this issue, or go to the journal homepage for more

Download details:

IP Address: 134.148.10.12
This content was downloaded on 01/01/2017 at 15:20

Please note that terms and conditions apply.

You may also be interested in:

Soccer ball lift coefficients via trajectory analysis
John Eric Goff and Matt J Carré

The effect of spin in swing bowling in cricket: model trajectories for spin alone
Garry Robinson and Ian Robinson

Particle-image velocimetry investigation of the fluid-structure interaction mechanisms of a natural owl wing
A Winzen, B Roidl and W Schröder

Effects of turbulence on the drag force on a golf ball
Rod Cross

The motion of an arbitrarily rotating spherical projectile and its application to ball games
Garry Robinson and Ian Robinson

Influence of light sheet separation on SPIV measurement in a large field spanwise plane
J M Foucaut, S Coudert, C Braud et al.

Spin-bowling in cricket re-visited: model trajectories for various spin-vector angles
Garry Robinson and Ian Robinson

IOP Publishing European Journal of Physics
Eur. J. Phys. 38 (2017) 024001 (16pp) doi:10.1088/1361-6404/aa51ea

Lift crisis of a spinning table tennis ball

T Miyazaki[1], W Sakai[1], T Komatsu[1], N Takahashi[2] and R Himeno[3]

[1] University of Electro-Communications, 1-5-1 Chofugaoka, Chofu, Tokyo, Japan
[2] Tokyo Denki University, 5 Senjuasahicho, Adachi-ku, Tokyo, Japan
[3] Institute of Physical and Chemical Research, 2-1 Hirosawa, Wako, Saitama, Japan

E-mail: miyazaki@miyazaki.mce.uec.ac.jp

Received 15 August 2016, revised 11 November 2016
Accepted for publication 6 December 2016
Published 29 December 2016

Abstract

The aerodynamic properties of a spinning table tennis ball were investigated using flight experiments. Using high-speed video cameras, the trajectory and rotation of an official ball (Nittaku 3-Star Premium), which was launched by a three rotor machine, were recorded. The drag and lift coefficients (C_D and C_L) were determined by analysing the video images. The measurements covered the speed and rotation range of typical table tennis shots in the form of the Reynolds number (Re) and dimensionless spin rate (SP), i.e. $3.0 \times 10^4 < Re < 9.0 \times 10^4$ and $0 < SP < 1.0$, and C_D and C_L were obtained as functions of Re and SP. We determined that the lift coefficient C_L is not a monotonically increasing function of SP. A deep valley of C_L was found around $SP = 0.5$, and the lift force exerted on a spinning ball almost vanished at $Re = 9.0 \times 10^4$ and $0.48 < SP < 0.5$. These results qualitatively agree with the results from recent wind tunnel tests, but quantitative differences owing to the unsteady nature of the flight experiments remain. This anomaly in the lift coefficient should be called the 'lift crisis'.

Keywords: aerodynamics, lift, drag, table tennis ball, flight experiments

(Some figures may appear in colour only in the online journal)

1. Introduction

An official table tennis ball is a sphere of diameter $d = 3.98$ cm with a mass $m = 2.74$ g that is made of celluloid (or plastic). In table tennis, the maximum velocity reaches to approximately 35 m s^{-1} (smash shot) and the maximum rotation rate to approximately 150 rps (heavy drive shot). Thus, the Reynolds number ($Re = \rho dU/\mu$) reaches to approximately 10^5 and the dimensionless spin rate ($SP = \pi d\omega/U$) to approximately 2. Here ρ and μ are the fluid density

and viscosity, respectively; U denotes the velocity of the ball and ω denotes the rotation rate. The aerodynamic force exerted on a table tennis ball is much greater than the gravitational force (mg, where g is the gravitational acceleration) because table tennis balls are very light; this is in contrast to balls used in other sports, which are far heavier. Therefore, it is of fundamental importance to sports science to investigate the aerodynamic properties of a lightweight spinning sphere, which is a simple bluff body. One might think that such a fundamental issue in fluid dynamics would have already been repeatedly and thoroughly studied. However, to our surprise, spinning spheres have escaped a systematic, quantitative study of their aerodynamic properties until very recently, probably because the Re range below 10^5 is of little interest from an engineering point of view. In contrast, the Re and SP ranges of table tennis shots is very interesting from a physicist's point of view because it overlaps with the range of the negative Magnus force reported in several previous research works. If negative Magnus force were exerted on a spinning table tennis ball, players would be very confused as they would observe that their drive (top-spin) shots would never drop and instead may even rise.

The Re–SP parameter region of negative Magnus force was first clarified by Taneda (1957). In his water tank tests, a spinning sphere was towed in still water and the direction of the exerted lateral force was determined by observing its lateral movement. A negative Magnus force was observed in the range $6 \times 10^4 < Re < 5 \times 10^5$ and $0 < SP < 0.6$. Briggs (1959) ascertained the occurrence of a negative Magnus force by dropping a spinning ball in a wind tunnel. Recently, Muto *et al* (2012) conducted large eddy simulations and found that the lift coefficient was negative ($C_L = -0.25$) at $Re = 2.0 \times 10^5$ and $SP = 0.2$. Kim *et al* (2014) carried out systematic wind tunnel experiments in a considerably wider parameter region ($6 \times 10^4 < Re < 1.8 \times 10^5$ and $0 < SP < 1.8$) and provided quantitative values of the drag and lift coefficients. The reported parameter range of the negative Magnus force was narrower than the range determined by Taneda. Konishi *et al* (2013) also carried out a wind tunnel test using a large table tennis ball (diameter 4.4 cm) in the lower Re range. Their results agreed very well with Taneda's negative Magnus force region. Moreover, the experimentally determined parameter ranges of the negative Magnus force overlap with those of table tennis shots. By performing free flight experiments, Tanaka *et al* (2014) tried to confirm the occurrence of a negative Magnus force in actual table tennis games. In their experiments, however, no negative Magnus force was observed in the parameter ranges $2.0 \times 10^4 < Re < 9.0 \times 10^4$ and $0 < SP < 1.0$, although a deep valley of C_L was found around $SP = 0.5$. The accuracy in determining the ball trajectory in their flight tests was not high enough to give the accuracy of C_D and C_L to within two significant figures. Thus, it has remained unclear whether their results were reliable, especially at high Reynolds numbers. More accurate measurements were required to explore the physical cause underlying the discrepancies between the previous experimental results.

The objective of this paper is to reinvestigate the aerodynamic properties of a spinning table tennis ball using flight experiments to obtain more accurate results. We covered the parameter ranges $3.0 \times 10^4 < Re < 9.0 \times 10^4$ and $0 < SP < 1.0$. The trajectory and rotation were recorded by high-speed video cameras, and the lift and drag coefficients were determined by analysing the video images. In the following section, the experimental apparatus is described. In section 3, the data processing method is explained and the results are presented in section 4. The comparison between the present results and those of the wind tunnel tests by Kim *et al* and Konishi *et al* is described in section 5. The last section is devoted to a brief summary of the results.

Figure 1. Left unmarked and right marked table tennis ball (Nittaku 3-Star Premium).

Figure 2. Three rotor launching machine 'Chiquita'.

2. Experimental apparatus

An official table tennis ball Nittaku 3-Star Premium made of celluloid was used in the present flight experiments; its diameter d was 39.8 mm with a standard deviation 0.76×10^{-2} mm (20 surface points $\times$ 10 balls), which is equivalent with the ball's surface roughness of about 0.2×10^{-3}. The mass m was 2.74 g with a standard deviation 1.50×10^{-2} g (100 balls). The ball was marked so that its rotation could easily be observed (see figure 1).

The ball was launched by a three rotor machine that was developed by JISS (Japan Institute of Sports Sciences) and Sunaga Development Co, Ltd to reproduce any table tennis shots used in actual games, including the 'Chiquita' backhand receive, with a very high spin rate (figure 2). The launching machine has three rotors of diameter 15.2 cm with a maximum rotation rate of 80 rps, and the rotors are able to inversely rotate as well. The maximum speed of the launched ball can reach 60 m s^{-1} with a maximum spin rate of 600 rps. In the present flight experiments, we launched a back spinning ball in the parameter ranges $3.0 \times 10^4 < Re < 9.0 \times 10^4$ and $0 < SP < 1.0$. The trajectory of a back spinning ball was relatively flat and remained in the centre region of the camera's frame, which improved the accuracy in determining the ball's position. The rotation rate is determined from the time during which the ball completes three revolutions. After every 20 shots, we changed the test

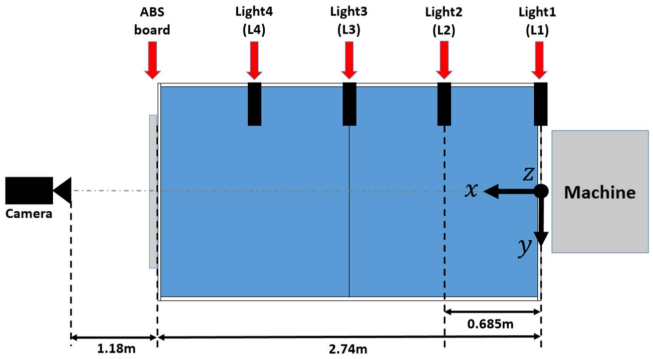

Figure 3. Experimental apparatus for the front camera recording.

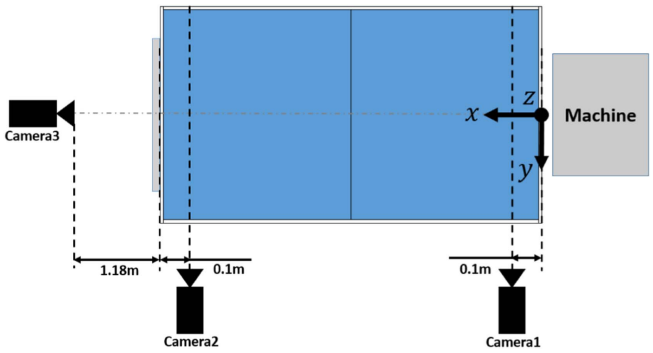

Figure 4. Experimental apparatus for the side camera recordings.

ball to a new one in order to keep the surface conditions as identical as possible. We used about 1200 balls in the present experiments.

Two types of experimental layouts were used in this study, as shown in figures 3 and 4. In the first arrangement, a single high-speed camera (Phantom Miro LC310, Vision Research) was placed in the plane of the ball's trajectory; it recorded front views of the vertical displacement of the ball. The ball was launched along the centre line of an official table (NT-3200, Nittaku) used in actual games. The coordinate origin was the launching point. The x-coordinate was the centre line of the table and the z-coordinate the vertical direction. A transparent acrylic board was placed at the other end ($x = 2.74$ m) of the table to stop the ball. The high-speed camera was located $l = 1.18$ m behind the board. A slit light sheet at $x = 0$ m, whose width was 3 mm, and three laser light sheets at $x = 0.685$, 1.37 and 2.055 m, of width 2 mm, illuminated the ball when it crossed these sheets. From the recorded video image, we could determine the time points (five in total) at which the ball passed these light sheets and hit the acrylic board. It is a major experimental refinement to use light sheets that had narrower widths in comparison with the sheets used in the experiments by Tanaka *et al* (2014) in which four slit light sheets (8 mm in width) from metal halide lamps were used. The frame rate of the high-speed camera was increased from 3000 fps ($Re = 3.0-6.0 \times 10^4$) to 4500 fps ($Re = 7.0-9.0 \times 10^4$) as the Reynolds number was increased. This is the second improvement on the previous measurements by Tanaka *et al* (2014) in which the frame rate was fixed to 1901 fps, irrespective of the Re number. Additionally, we increased the number

of data points N in determining the ball trajectory, which was 20 in the measurements by Tanaka *et al* (2014). Here, for the Reynolds number range $Re = 3.0{-}5.0 \times 10^4$, N was 50, while N was slightly decreased to $N = 40$ for $Re = 6.0{-}9.0 \times 10^4$ because the ball reached the board faster.

The second experimental arrangement is illustrated in figure 4. In addition to the front camera, two high-speed cameras, located 2.54 m apart, recorded two side views of the ball at 4500 fps. The front camera was used to record the sideward deviation of the ball trajectory from the centre line. When no lift force is exerted on the ball, we can determine the drag coefficient from the ratio of the horizontal velocity component determined at the two cameras' positions. The details of the data analysis are explained in the next section. The second method was used to check the accuracy of the first method in determining the drag coefficient.

3. Method of data analysis

The data analysis procedure is explained in this section. From the camera images, we know the five times T_1, T_2, T_3, T_4 and T_5, at which the ball is located at the five fixed positions $x_1 = 0$ m, $x_2 = 0.685$ m, $x_3 = 1.37$ m, $x_4 = 2.055$ m and $x_5 = 2.74$ m. Also, analysing the camera images, i.e. reading the pixel data $z_p(t_j)$ of the ball centre, we determine $z(t_j)$ at N times $t_1, t_2, \ldots, t_N$. We have to convert the pixel data to the z-coordinate using the following linear relation $z(t_j) = \Delta(l + x_5 - x(t_j))/l$. Here, the length scale is calibrated at the board x_5, as $\Delta = 0.844$ mm/pixel and $x(t_j)$ denotes the x-coordinate of the ball centre at the time $t = t_j$, which is estimated by interpolating the above five times T_{1-5} at which the ball centre crosses the five fixed positions x_{1-5}. The interpolation procedure based on the numerical computation will be explained below in detail.

We fitted the recorded ball trajectories with numerically computed ones. In our numerical computations, we assumed that the drag and lift coefficients were constant throughout each flight. The actual data fitting process consists of the following two steps. First, we get a rough estimate of the drag and lift coefficients using an approximate solution of the equations of motion. The resulting rough estimate is used as an initial guess for the starting conditions of a numerical iteration procedure in the second step.

The basic equations of motion are given as follows:

$$\frac{\mathrm{d}x}{\mathrm{d}t} = u, \tag{1}$$

$$\frac{\mathrm{d}z}{\mathrm{d}t} = w, \tag{2}$$

$$\frac{\mathrm{d}u}{\mathrm{d}t} = -\frac{1}{2}Du\sqrt{u^2 + w^2} - \frac{1}{2}Lw\sqrt{u^2 + w^2}, \tag{3}$$

$$\frac{\mathrm{d}w}{\mathrm{d}t} = -g - \frac{1}{2}Dw\sqrt{u^2 + w^2} + \frac{1}{2}Lu\sqrt{u^2 + w^2}. \tag{4}$$

Here, u denotes the horizontal velocity component and w the vertical velocity component. We introduce two coefficients $D = \rho\pi d^2 C_\mathrm{D}/4\,m$ and $L = \rho\pi d^2 C_\mathrm{L}/4\,m$ instead of C_D and C_L for convenience in later calculations. The trajectory of a back spinning ball remains in a vertical plane because no side force is exerted on it. The buoyancy, which is less than 1.5% of the gravitational force mg, is not taken into account.

We have the following approximate solution $x = x_0(t)$; by assuming that the ball trajectory is a straight horizontal line, i.e. assuming $w = 0$, we find that

$$x_0(t) = \frac{2}{D}\log\left(1 + \frac{u_0 Dt}{2}\right). \tag{5}$$

Here, u_0 and D denote the initial velocity and the velocity decay rate, which is to be determined. From the camera image S, we know the five times t_1, t_2, t_3, t_4 and t_5, at which the ball is located at the five fixed positions $x_1 = 0$ m, $x_2 = 0.685$ m, $x_3 = 1.37$ m, $x_4 = 2.055$ m and $x_5 = 2.74$ m. We are able to obtain rough estimates for u_0 and D, based on a least squares method by minimising the deviation between the experimental data and the approximate theoretical values $x_0(t_i)$ from (5) according to the following equation:

$$\sum |x_i - x_0(t_i)|^2. \tag{6}$$

Next, we consider the vertical component. We have an approximate series solution of (2) and (4), which is given by

$$z \approx z_0 + w_0 t + \left(\frac{-g}{2} + \frac{L{u_0}^2}{4} - \frac{D^2{u_0}^2 w_0}{4}\right)t^2 + \left(\frac{D^2{u_0}^2 w_0}{12} - \frac{DL{u_0}^3}{8} + \frac{5Dgu_0}{12}\right)t^3. \tag{7}$$

Here, w_0 denotes the initial value of the vertical velocity component and L is the factor proportional to the lift coefficient. Analysing the camera images, i.e. reading the pixel data of the ball centre, we determine $z(t_j)$ at N times $t_1, t_2, \ldots, t_N$. It should be noted that we use the above approximate estimate $x_0(t_j)$ in converting the pixel data to the vertical position $z(t_j)$. Again utilising a least squares method, we obtain rough estimates for w_0 and L. These estimates are used as an initial guess for the next step.

In the second step, we integrate the equations of motion (1)–(4) numerically starting from the approximate initial values for u_0 and w_0 with the approximate estimates for D and L. The least squares method for the trajectory fitting is utilised to provide a better guess for u_0, w_0, D and L at each step, and we continue the iteration procedure to arrive at well converged values for u_0, w_0, D and L. In the iteration procedure, we use the time information at the five fixed positions as the constraints, so that the timing error should never exceed a half frame time.

As can be seen below, the iteration procedure converged rapidly in the parameter region, where D and L depended weakly on Re and SP. The residuals in fitting the ball position (z-coordinate) were less than 1 mm for a well converged case. We obtained C_D and C_L from D and L, using the relations $C_\mathrm{D} = 4\,mD/\rho\pi d^2$ and $C_\mathrm{L} = 4\,mL/\rho\pi d^2$, respectively.

The assumption that the drag and lift coefficients are constant throughout each flight is not strictly satisfied because the velocity decays by more than 25% while the rotation rate remains almost constant, which means that Re decreases by 25% and SP increases by 25%. Thus, the flight of a table tennis ball is essentially an unsteady fluid dynamical problem. If the drag and lift coefficients depend significantly on Re and/or SP, then we cannot assume that they are constant during each flight. In addition, there might be some truly unsteady contributions to the aerodynamics, such as a memory effect in the unsteady Stokes problem. Therefore, we must be careful when discussing the obtained results and keep the above mentioned points in mind. We will come back to this important issue in section 5.

The method of data analysis using the side view images is much simpler, because we have an analytical solution of (1)–(4) if no lift force is exerted on the ball, i.e. $L = 0$ ($C_\mathrm{L} = 0$). We introduce the length s along the ball trajectory, whose derivative with respect to

time is given by

$$\frac{\mathrm{d}s}{\mathrm{d}t} = \sqrt{u^2 + w^2}. \tag{8}$$

Dividing (3) by (8), we have a new linear equation:

$$\frac{\mathrm{d}u}{\mathrm{d}s} = -\frac{1}{2}Du. \tag{9}$$

This equation is integrated to yield,

$$u = u_0 \ \exp\left(-\frac{1}{2}Ds\right). \tag{10}$$

Note that D is directly related to the horizontal velocity component according to

$$D = -\frac{2}{s}\ln\left(\frac{u_0}{u}\right). \tag{11}$$

We can approximate the length s along the trajectory by the difference in the x-coordinate fairly well since the trajectory is almost straight in the Re number range considered in this study. The horizontal velocity components at the two points can be determined from the video images of the two side cameras. They were determined by knowing the times during which the ball moved 10 cm at the two points. However, we must make a slight correction when the ball trajectory deviates from the centre line of the table, where the length scale of the image is calibrated. The details of the data correction are explained in Miyazaki *et al* (2013), who determined the drag coefficient of an archery arrow using the same data correction procedure.

4. Results

We explain the results of the flight experiments in this section. First, we check the accuracy of our measurement procedure for several parameter values. We repeated the flight experiments about 30 times at each parameter set of Re and SP and computed the mean value with the standard deviation of the drag and lift coefficients. In addition, we performed side view analyses at the parameter sets for which no lift force was exerted.

4.1. Accuracy of front view experiments for rotating shots with SP > 0.0

We list the results of the accuracy check in table 1, where the previous results given by Tanaka *et al* (2014) are added for comparison. In general, the obtained lift coefficient C_L seems fairly accurate with a small standard deviation. The relative error at $Re = 4.0 \times 10^4$ and $SP = 1.0$ is about 3%. The lift coefficient almost vanishes at $Re = 9.0 \times 10^4$ and $SP = 0.5$, where the minimum value $C_\mathrm{L} = -0.005$ is obtained. The present results for the lift coefficient agree fairly well with those of Tanaka *et al* (2014) even at higher Reynolds numbers. In contrast, the present measurements provide significantly smaller values for the drag coefficient C_D. This tells us that the improvements in the experimental set-up can reduce the errors in the determination of the five time points T_1, …, T_5 and refine the accuracy in determining the drag coefficient.

Table 1. Drag and lift coefficients from the front camera measurements at $Re = 4.0 \times 10^4$, $SP = 1.0$ and $Re = 9.0 \times 10^4$, $SP = 0.5$. Bold letters: mean value; [ ]: standard deviation; (): number of shots.

	C_D $Re = 4.0 \times 10^4$ $SP = 1.0$	C_L $Re = 4.0 \times 10^4$ $SP = 1.0$	C_D $Re = 9.0 \times 10^4$ $SP = 0.5$	C_L $Re = 9.0 \times 10^4$ $SP = 0.5$
Tanaka *et al* (2014)	**0.480** [0.008] (28)	**0.306** [0.014] (28)	**0.398** [0.011] (30)	**0.028** [0.032] (30)
Present study	**0.419** [0.009] (24)	**0.322** [0.010] (24)	**0.324** [0.012] (31)	**−0.005** [0.018] (31)

Table 2. Drag coefficient from the front and side camera measurements at $Re = 4.0 \times 10^4$, $SP = 0.0$ and $Re = 9.0 \times 10^4$, $SP = 0.48$. Bold letters: mean value; [ ]: standard deviation; (): number of shots.

	C_D (Front camera) $Re = 4.0 \times 10^4$ $SP = 0.0$	C_D (Side cameras) $Re = 4.0 \times 10^4$ $SP = 0.0$	C_D (Front camera) $Re = 9.0 \times 10^4$ $SP = 0.48$	C_D (Side cameras) $Re = 9.0 \times 10^4$ $SP = 0.48$
Tanaka *et al* (2014)	**0.456** [0.008] (28)	**0.444** [0.021] (25)	No data	No data
Present study	**0.421** [0.008] (33)	**0.421** [0.018] (30)	**0.354** [0.017] (29)	**0.358** [0.016] (50)

4.2. Accuracy of side view experiments for a non-rotating shot with SP = 0.0 and for the case Re = 9.0 × 10⁴, SP = 0.48

Next, let us check the accuracy of the measured drag coefficient. Table 2 (the two left-most columns) compares the results from the two experimental set-ups (i.e. front and side views) for a non-rotating shot with $SP = 0.0$ at $Re = 4.0 \times 10^4$. The previous results for a non-rotating ball by Tanaka *et al* (2014) are listed as well. We note that the present drag coefficient at $Re = 4.0 \times 10^4$ and $SP = 0.0$ is smaller than the previous value by 7%. It is also noted that the two measurements provided the same value of $C_D = 0.421$ in the present study, whereas a deviation of about 3% was found between the results by Tanaka *et al* (2014). In addition, we carried out a side view measurement of C_D at $Re = 9.0 \times 10^4$ and $SP = 0.48$ where almost no lift force was exerted on the ball, and found good agreement within about 1% (table 2: the two right-most columns). The front view value is 0.354 and the side view value is 0.358, confirming the accuracy of the present measurements.

4.3. Results of the flight tests

Figure 5 shows the drag and lift coefficients for $SP = 0.5$ and 1.0 as functions of Re. The horizontal axis denotes the Reynold number and the vertical axis denotes C_D and C_L. Both the drag and lift coefficients for $SP = 0.5$ decrease monotonically with Re in the range

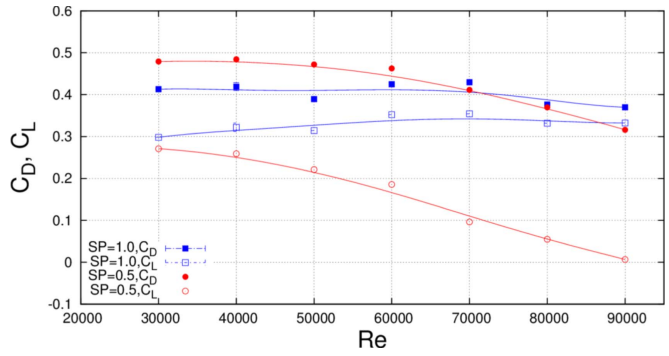

Figure 5. C_{D} (closed symbols) and C_{L} (open symbols) as functions of Re for $SP = 0.5$ and 1.0.

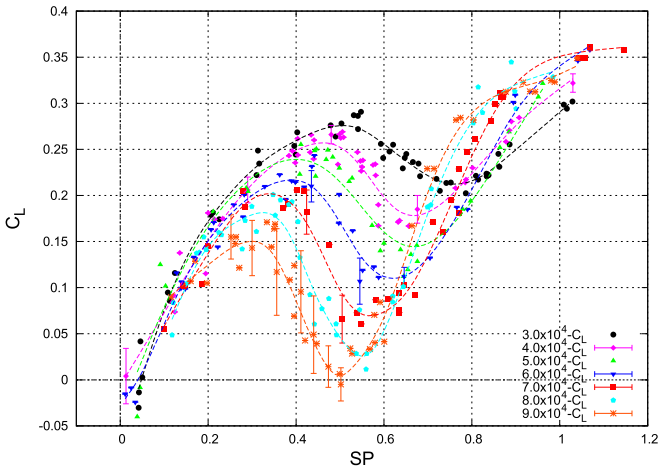

Figure 6. Lift coefficient as a function of SP.

$Re > 5.0 \times 10^4$. It should be noted that C_{L} (red open circles) decreases to zero and that C_{D} (red closed circles) goes to about 0.32 at $Re = 9.0 \times 10^4$, suggesting the occurrence of the negative Magnus force at higher Reynolds numbers. In contrast, the drag and lift coefficients for $SP = 1.0$ (C_{D}: blue closed squares and C_{L}: blue open squares) vary moderately around the constant values $C_{\mathrm{D}} = 0.4$ and $C_{\mathrm{L}} = 0.33$, respectively.

The main results of the flight tests are presented in figures 6 and 7, where the variations of C_{L} and C_{D} with respect to the spin parameter SP are illustrated for the Reynolds numbers $Re = 3.0 \times 10^4$, 4.0×10^4, …, 9.0×10^4. The horizontal axis shows SP and the vertical axis C_{L} and C_{D}. The parameters Re and SP are defined by the initial values of the velocity and the rotation rate. It should be noted that the velocity decreases by about 25%, whereas the rotation rate remains almost constant (within 2%). Then, the instantaneous Reynold number Re decreases and the instantaneous spin parameter SP increases during each flight. We will discuss this issue in more detail in section 5.

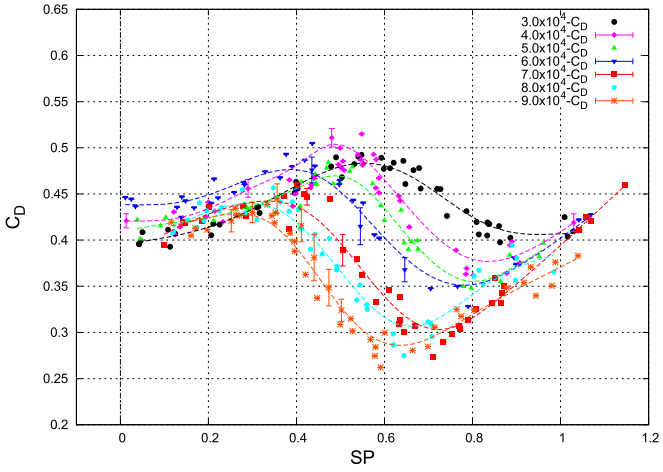

Figure 7. Drag coefficient as a function of SP.

First, we look at the dependence of the lift coefficient C_L on SP. For small SP values less than 0.3, C_L increases linearly with respect to SP, irrespective of Re, whose gradient is estimated to be about 0.8. This linear increase of C_L with SP, however, saturates and the lift coefficient attains its maximum value C_{Lmax} at SP_{max}. It is interesting to see that C_L decreases and attains its minimum C_{Lmin} at SP_{min} if SP is increased further. The lift coefficient is not a monotonically increasing function of the rotation rate SP. Both the maximum and minimum values C_{Lmax} and C_{Lmin} become smaller as the Reynolds number increases. In the recent wind tunnel experiments by Kim *et al* and Konishi *et al*, a corresponding decrease in C_L was observed along with a discontinuous jump from C_{Lmax} to C_{Lmin}, indicating the sudden occurrence of a laminar to turbulent transition of the lower boundary layer. In contrast, the lift coefficient obtained in the present flight tests, which is an averaged value during a 2.74 m flight, shows continuous variation even in the range $SP_{max} < SP < SP_{min}$. As Re is increased, C_L decreases sharply and a deeper valley is formed. We have already noted that C_{Lmin} vanishes at $Re = 9.0 \times 10^4$ and $0.48 < SP < 0.5$, i.e. almost no lift force is exerted on the ball. In fact, we have occasionally observed negative C_L values around $Re = 9.0 \times 10^4$ and $SP = 0.5$, but they are within the fluctuations of our measurements. In figure 6, the standard deviation is shown by an error bar at several SP values for Re values of 4.0×10^4, 6.0×10^4, 7.0×10^4 and 9.0×10^4. We note that the standard deviation becomes large around SP_{max} at $Re = 9.0 \times 10^4$. We discuss this finding in the next section in detail. As SP is increased further, the lift coefficient tends to increase further with SP and the dependence on Re for $SP > SP_{min}$ becomes weak again.

The lift coefficient seems to collapse approximately on two different curves, i.e. $0.82\ SP - 0.58\ SP^2$ for $SP < SP_{max}$ and $-0.58 + 1.37\ SP - 0.44\ SP^2$ for $SP > SP_{min}$, respectively. The decrease of C_L with SP might be considered to be a transition from the former branch to the latter branch that takes place at smaller SP as Re increases. There exists a parameter range in the Re–SP plane where the lift coefficient sensitively depends on two parameters. As already noted, the physical mechanism of this sensitive dependence is the laminar to turbulent transition of the boundary layer on the lower surface, which occurs at smaller SP for larger Re. The present results seem to be qualitatively in accordance, but quantitatively inconsistent, with both of the results from the recent wind tunnel tests by Kim *et al* (2014) and Konishi *et al* (2013). The negative Magnus force is not found in the

parameter range of table tennis shots. We will compare our results with theirs in the following section and discuss the reason for the discrepancy.

Next, we examine the variations of the drag coefficient C_D. The general trend is similar to that of the lift coefficient. For small SP below SP_{max}, the drag coefficient increases slightly with SP. When SP exceeds SP_{max}, the drag coefficient decreases with SP, corresponding to the shrink of the wake width associated with the boundary layer transition. The drag coefficient C_D attains its minimum C_{Dmin} at SP_{Dmin}, where the wake is narrowest. The value of SP_{Dmin} is larger than SP_{min} at all Reynold numbers considered in this study. As in the lift coefficient, the drag coefficient seems to collapse on two different lines, i.e. $0.41 + 0.09\ SP + 0.12\ SP^2$ for $SP < SP_{max}$ and $0.25 - 0.12\ SP + 0.27\ SP^2$ for $SP > SP_{Dmin}$, respectively. A transition from the former branch to the latter branch at each Re can be seen, just as for the lift coefficient C_L. Although the decrease in the C_D value is more moderate and less drastic (within 50%), it might have a non-negligible influence in actual games since the time for a ball to fly across the table is considerably reduced.

The mechanism of these variations in the aerodynamic coefficients was first explained by Taneda (1957), whose explanation was supported by a beautiful visualisation in the recent wind tunnel experiments by Kim *et al* (2014). They showed the separation points (lines) and the streamlines using digital particle image velocity measurements (although the Reynolds numbers 1.0×10^5 and 1.4×10^5 were higher than those of table tennis shots). The abrupt decrease of the lift coefficient is certainly linked with the laminar to turbulent transition of the lower boundary layer and the resulting delay of the main separation. The stronger local shear in the lower surface induces instability and a transition to turbulence, while the upper surface remains laminar. When Re increases, this asymmetric transition occurs at lower SP. Even if the lift coefficient does not cross the zero line, this drastic change in C_L should be called the 'lift crisis', since its mechanism is quite similar to that of the 'drag crisis' of a non-rotating sphere (see e.g. Schlichting 1979).

5. Discussions

The present results are compared quantitatively with those of the recent wind tunnel measurements by Kim *et al* (2014) and Konishi *et al* (2013) in this section. Figures 8 and 9 show the drag (solid lines) and lift coefficients (dashed lines) as functions of SP at Re values of 6.0×10^4 and 8.0×10^4, respectively. The red and blue lines show the results by Kim *et al* (2014) and Konishi *et al* (2013), respectively. The black and grey lines are our results. Note that our results differ from the literature results. Let us consider the reason for these inconsistencies. There are several factors influencing the boundary layer transition in the wind tunnel tests, such as the surface condition of the ball, supporting system of the rotating ball and upstream turbulence intensity. There is also a crucial difference between the wind tunnel tests and the present free flight tests. The free flights are essentially unsteady fluid dynamical phenomena with a large deceleration, whereas the wind tunnel tests are conducted in steady environments. We will see below that the unsteadiness is the main cause of the differences.

First of all, the results from the two wind tunnel tests do not coincide quantitatively, although qualitatively they do show a similar dependence on SP. As SP is increased, the lift coefficient increases to a maximum value and it jumps suddenly to a minimum and then increases again. The critical SP value reported by Konishi *et al* (2013) (blue dashed lines), where the jump occurs, is substantially smaller than that reported by Kim *et al* (2014) (red dashed lines). We suspect that this difference is mainly caused by the difference in the surface roughness. Konishi *et al* used a large table tennis ball, whereas Kim *et al* used a smooth

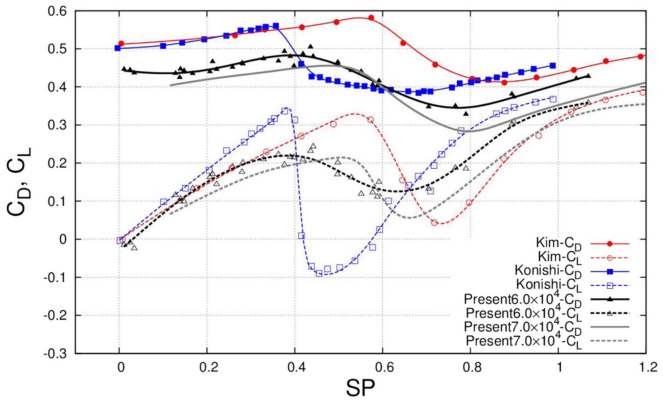

Figure 8. The drag and lift coefficients as functions of *SP* at $Re = 6.0 \times 10^4$. Comparison with previous wind tunnel tests.

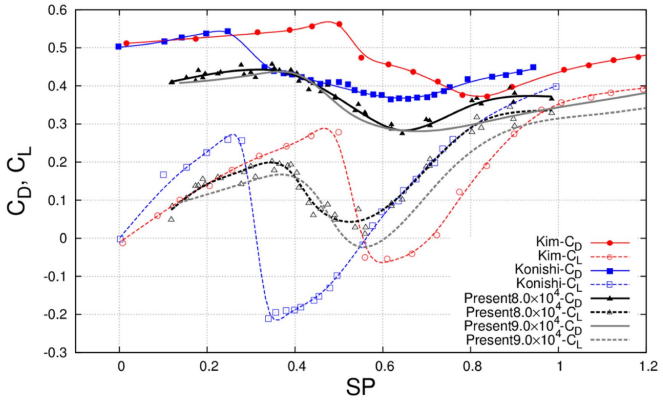

Figure 9. The drag and lift coefficients as functions of *SP* at $Re = 8.0 \times 10^4$. Comparison with the previous wind tunnel tests.

sphere made of acrylonitrile butadiene styrene resin. It is reasonable to think that the boundary layer transition took place at considerably smaller *SP* in Konishi *et al*'s experiments owing to the surface roughness. In the present flight experiments, we launched an official table tennis ball with the same (or at least similar) roughness. Then, our results (black dashed lines) might be expected to agree more with those of Konishi *et al* (2013), but there are still significant deviations.

Next, we should remember that the velocity of a launched ball decreases by about 25% when it reaches the acrylic board, whereas the rotation rate does not decrease in the flight experiments. Thus, *Re* decreases by 25% and *SP* increases by 25% during each flight of a ball. If we redefine these parameters using the averaged value of the velocity, Re_{av} is reduced by 15% and SP_{av} is increased by 15%. A better comparison with the results from the wind tunnel tests might be found if we used these averaged parameter values instead of those estimated from the initial values. We replot our results at *Re* values of 7.0×10^4 and 9.0×10^4 (corresponding Re_{av} values of 6.0×10^4 and 7.7×10^4), indicated by the grey lines in figures 8 and 9, where the horizontal axis is SP_{av}. The grey solid and dashed lines are drawn

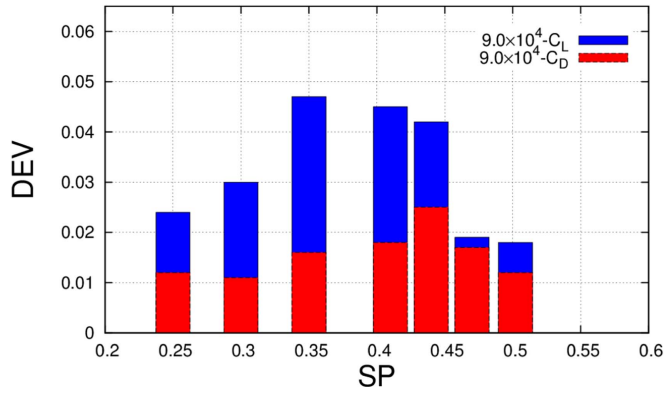

Figure 10. Standard deviations of C_L and C_D as functions of SP at $Re = 9.0 \times 10^4$.

fairly close to the original plots (black solid and dashed lines) and the deviations are not remedied by such simple changes of the parameter definitions, suggesting that we need to search for a more fundamental reason for these inconsistencies.

One may speculate whether the sharp jump of the lift coefficient around $SP = 0.35$ observed in the wind tunnel test may be the crucial cause of this difference. Actually, such sharp jumps are inevitably smoothed out in the data analysis of our flight tests. We assume that the drag and lift coefficients remain constant in each flight experiment, which might be an over-simplification of the unsteady phenomena around the critical parameter value of $SP = 0.35$. We repeated the flight experiments (40 shots) at $Re = 9.0 \times 10^4$ and $SP = 0.35$, resulting in more than half the trajectories being poorly fitted by our data analysis procedure. In addition, even in the successfully fitted cases, the obtained C_L widely fluctuates, as demonstrated by the large error bar ($C_L = 0.12 \pm 0.047$) in figure 6. We note the presence of a critical phenomenon when studying the statistical nature around SP_{max} more carefully. We show in figure 10 the standard deviations of C_L and C_D as functions of SP at $Re = 9.0 \times 10^4$. At each SP, we repeat the flight experiments more than 30 times in order to provide the mean value with the standard deviation (see the plot in figure 6 for the mean value). The standard deviation of C_L (blue) has a clear hump in the range $0.25 < SP < 0.45$, while that of C_D (red) shows a weak dependence on SP. This observation provides further evidence for the occurrence of the 'lift crisis', in which the lift force exerted on the ball widely fluctuates and becomes indeterminate because of the delicate nature of the laminar–turbulent transition. Table tennis players might not be confident of the repeatability of their shots in the 'lift crisis' zone.

However, there still remain non-negligible differences between the C_L values from the wind tunnel tests and those of our flight tests. The results of the present flight tests do not support the occurrence of the negative Magnus force throughout the parameter range considered, while negative values of C_L below -0.2 were obtained around $SP = 0.4$ and $Re = 8.0 \times 10^4$ by Konishi *et al* (2013). Recently, Konishi *et al* (2014, 2016) conducted preliminary flight experiments. They compared the trajectories in their flight experiments with those computed using the instantaneous C_D and C_L values interpolated from the data of their wind tunnel tests to find out qualitative differences in the specified parameter ranges.

With regards to these findings, Taneda (1957) pointed out another important unsteady nature of the phenomena. A considerably long run-up length was required (more than 50 times the diameter of the sphere) to generate a negative Magnus force in his towing tank

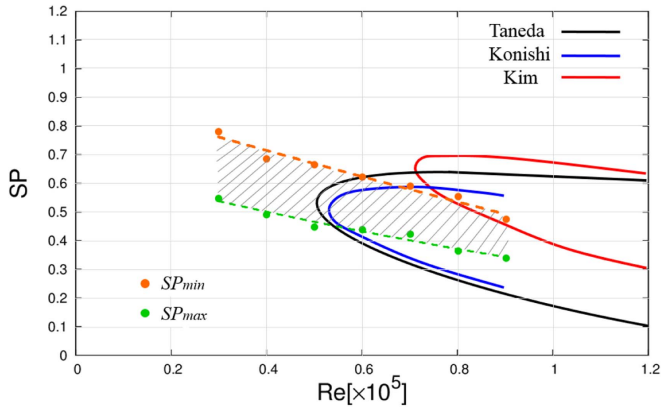

Figure 11. The parameter region of the negative Magnus effect.

experiments. A positive Magnus force was always exerted within the run-up length. In the present flight experiments, the corresponding run-up length was about 2 m (over $2/3$ of the whole trajectory). The laminar–turbulent transition may not take place in the flight experiments, even if the wind tunnel tests predict its occurrence. The boundary layer transition is less likely to take place in the flight experiments and the 'lift crisis' zone shifts to the larger *SP* range. It is important to investigate the unsteady aspect of the 'lift crisis' in more detail, as in the case of the 'drag crisis'. We tried to estimate the instantaneous values of aerodynamic properties by twice differentiating the z-coordinate with respect to time, thereby finding a large unphysical fluctuation of the lift coefficient caused by the inaccuracy in determining the ball position (about 1 mm). If the accuracy were increased by one order of magnitude, i.e. to 0.1 mm, it would be possible to obtain reasonable instantaneous values of the drag and lift coefficients; this will be the topic of future work.

Figure 11 summarises the parameter region on the *Re*–*SP* plane, where the negative Magnus force occurred in the wind tunnel experiments. The solid black line shows the result by Taneda (1957) and Konishi *et al* (2013) (blue line) reproduced almost the same threshold. The red line is the result given by Kim *et al* (2014), who predicted a narrower region of the negative Magnus force. We insert a hatched zone in which the lift coefficient C_{L} decreases with the spin rate *SP* in our flight measurements. It indicates the 'lift crisis' zone where C_{L} depends very sensitively on *Re* and *SP* with large fluctuations. The present results demonstrate that the negative Magnus force is unlikely to occur in table tennis games, but that the 'lift crisis' does occur in the parameter range where the negative Magnus force was observed by these wind tunnel and water channel tests. The Reynolds number and the spin parameter of a loop drive shot with the velocity 15.7 m s^{-1} and the rotation rate 125 rps, are known to be 4.0×10^4 and 1.0, respectively. If the velocity is doubled and the rotation rate is unchanged, as in a heavy drive shot, *Re* increases to 8.0×10^4 and *SP* is decreased to 0.5, just falling into this zone. Players whose shots have both a high velocity and high spin rate should be aware of the 'lift crisis' zone and steer clear of it.

Finally, as for the drag coefficient, we also note a smaller but still non-negligible difference between our values and the literature values even for a non-spinning ball ($SP = 0.0$). The previous wind tunnel tests gave a value of C_{D} of 0.5 but the present flight experiments gave $C_{\mathrm{D}} = 0.44$ with a standard deviation of about 0.01 for $4.0 \times 10^4 < Re < 9.0 \times 10^4$ (subcritical range). This difference is most likely caused by the large deceleration of the ball in free flight. The above mentioned difference in *Re* and Re_{av} cannot explain it because the C_{D}

of a non-spinning ball only depends very weakly on *Re*. The effect of the induced mass (half of the air mass of the ball volume) is estimated to contribute less than 1%, which is also insufficient to explain the difference. Thus, this difference can be attributed to the difference in the separation line on the ball surface caused by the large deceleration. The unsteady aspects remain to be explored, even in the subcritical *Re* range.

6. Summary

We have investigated the aerodynamic properties of a spinning table tennis ball using free flight experiments. The lift coefficient does not increase with *SP* monotonically, but a sharp decrease from a maximum to a minimum is observed at high *Re* numbers. Although the negative Magnus force is unlikely to occur in the parameter range of table tennis shots, the lift force almost vanishes at $Re = 9.0 \times 10^4$ and $0.48 < SP < 0.5$. These phenomena are linked to the asymmetry of the laminar to turbulent transition of the boundary layer flow. As the spin parameter *SP* increases, the boundary layer moving against the spinning ball surface becomes turbulent, while the boundary layer flow moving with the spinning ball surface remains laminar. The separation point moves downstream on the former (against-) side, which considerably reduces the lift force. We propose that this region should be referred to as the 'lift crisis', even if the lift coefficient does not jump to a negative value because the mechanism is quite similar to that of the 'drag crisis' of a non-rotating sphere.

The values of the lift coefficient obtained from the free flight tests differ quantitatively from those provided from the recent wind tunnel tests. We also note the inconsistencies between the results from previous wind tunnel experiments. Those are likely caused by the delicate nature of the boundary layer transition, which is caused by such factors as the high sensitivity to the turbulence intensity in the wind tunnels, to the surface roughness of the ball and also to the mechanical supporting system of the rotating ball. In addition, the unsteadiness in the flight experiments, i.e. 25% velocity deceleration, may have a substantial influence on the laminar to turbulent transition. Since any flow fields in sports games are inevitably unsteady, we must be very careful in predicting the trajectory of a ball in free flight based solely on the aerodynamic properties obtained from wind tunnel tests since those measurements are usually conducted in steady environments. An accurate flight test will certainly be required to give practical and useful predictions and to explore the unsteady aspects of sports fluid dynamics. Sports remind us that many unsolved problems still remain in the field of fluid dynamics.

Acknowledgments

We are grateful to Dr Ozaki of Japan Institute of Sports Sciences (JISS) and Sunaga Development Co., Ltd for their help in developing the launching machine 'Chiquita'. This work is supported by JISS's 'Team Japan Multi-support Project' entrusted from the Ministry of Education, Culture, Sports, Science and Technology. We are also grateful to Nittaku for providing an official table (NT-3200) and a number of official balls (Nittaku 3-Star Premium). The present flight tests could never be accomplished without their support.

References

Briggs L J 1959 Effect of spin and speed on the lateral deflection (curve) of a baseball and the Magnus effect for smooth spheres *Am. J. Phys.* **27** 589–96

Kim J, Choi H, Park H and Yoo J Y 2014 Negative Magnus effect on a rotating sphere: when and why *J. Fluid Mech.* **754** R2

Konishi Y, Okuizumi H and Ohno T 2014 A comparison of aerodynamic force of table tennis ball between wind tunnel experiment and a flight experiment *JSME Symp.: Sports and Human Dynamics* 2014, USB (in Japanese)

Konishi Y, Okuizumi H and Ohno T 2016 PIV measurement of a flying table tennis ball *Proc. 11th Conf. of the Int. Sports Engineering Association (ISEA) 2016, Proc. Eng.* **147** 104–9

Konishi Y, Okuizumi H, Ohno T and Obayashi S 2013 The measurement of the negative Magnus force on a table tennis ball *Proc. Symp. on Sports and Human Dynamics 2013* p 235 (in Japanese)

Miyazaki T, Mukaiyama K, Komori Y, Okawa Y, Taguchi S and Sugiura H 2013 Aerodynamic properties of an archery arrow *Sports Eng.* **16** 43–54

Muto M, Tsubokura M and Oshima N 2012 Negative Magnus lift on a rotating sphere at around the critical reynolds number *Phys. Fluids* **24** 014102

Schlichting H 1979 *Boundary Layer Theory* 7th edn (New York: McGraw-Hill)

Tanaka K, Fukujyu T, Miyazaki T and Himeno R 2014 Aerodynamic properties of a table tennis ball *Nagare* **33** 37–45 (in Japanese)

Taneda S 1957 Negative Magnus effect *Rep. Res. Inst. Appl. Mech.* **5** 123–8